# Role of resonance-enhanced multiphoton excitation in high-harmonic generation of N_{2}: A time-dependent density-functional-theory study

Xi Chu and Gerrit C. Groenenboom

Phys. Rev. A **87**, 013434 — Published 31 January 2013

DOI: 10.1103/PhysRevA.87.013434

# Role of resonance enhanced multiphoton excitation in high harmonic generation of $N_2$: A TDDFT study

Xi Chu

*Department of Chemistry and Biochemistry,*

*The University of Montana, Missoula, Montana 59812*

Gerrit C. Groenenboom

*Institute for Molecules and Materials,*

*Radboud University Nijmegen, Heyendaalseweg 135,*

*6525 AJ Nijmegen, The Netherlands*

(Dated: January 10, 2013)

## Abstract

A minimum at ∼39 eV is observed in the high harmonic generation (HHG) spectra of $N_2$ for several laser intensities and frequencies. This minimum appears to be invariant for different molecular orientations. We reproduce this minimum for a set of laser parameters and orientations in time dependent density functional theory calculations, which also render orientation dependent maxima at 23–26 eV. Photon energies of these maxima overlap with ionization potentials of excited states observed in photoelectron spectra. Time profile analysis shows that these maxima are caused by resonance enhanced multiphoton excitation. We propose a four step mechanism, in which an additional excitation step is added to the well accepted three step model. Excitation to the linear combination of Rydberg states $c_4' \, ^1\Sigma_u^+$ and $c_3 \, ^1\Pi_u$, gives rise to an orientation invariant minimum analogous to the "Cooper minimum" in argon. When the molecular axis is parallel to the polarization direction of the field, a radial node goes through the atomic centers, and hence the Cooper-like minimum coincides with the minimum predicted by a modified two-center interference model that considers the de-excitation of the ion and symmetry of the Rydberg orbital.

PACS numbers: 33.80.Rv,42.50.Hz,33.80.Eh,33.90.+h

## I. INTRODUCTION

Exciting results have been obtained in recent years by using HHG [1, 2] to probe molecular dynamics with subfemtosecond temporal resolution [3–8]. The sensitivity of HHG emission to molecular geometry and motion is the foundation for this application. In particular, minima in HHG spectra [7, 9] and the involvement of multiple ionization channels [10–12] may correlate with molecular structure and cause oscillation of the HHG intensity in response to geometry changes in molecules. Among different types of minima, those due to two-center interference [13] and Cooper minima initially observed in photoionization [14] and caused by radial nodes of the ground state wave function have attracted much attention. The HHG of $CO_2$ is well studied and believed to exhibit the two-center interference [13] type of minimum [15], whose position depends on the molecular orientation and parameters of the incident laser. Wörner *et al.* [16] concluded that two molecular orbitals (MOs) contribute to the HHG of $CO_2$, which leads to controllable phase differences. In contrast they also reported a minimum for $N_2$, which remains at $\sim$39 eV for different alignment angles and incident laser parameters. As such, it is considered to be Cooper-like. The HHG spectra of Ar [17, 18], Kr, and Xe [19] have been shown to exhibit Cooper minima, and it has been pointed out that the single active electron (SAE) model is not sufficiently accurate to determine the positions of the minima [20]. To confirm a Cooper minimum in a molecule is even less straightforward. An expansion of both the ground and continuum wave function into angular momentum space is needed. In the most recent work by Bertrand *et al.* [9], HHG measurements using a longer wavelength, 1200 nm, were compared to a SAE calculation involving only the highest occupied molecular orbital (HOMO). They concluded that the destructive interference between the recombination contributions from the $p$ and $f$ free electron partial waves gave rise to the minimum. The difference between theory and measurements, however, is as large as 13 eV.

It is generally accepted that HHG of $N_2$ is due to activity of the electron initially occupying the HOMO. The HOMO-1, on the other hand, has also been shown to influence the molecular orientation dependent intensity [21] and phase[11, 22] of HHG. Current strong field theory for HHG largely relies on the semiclassical Lewenstein model [23]. Semiclassical methods usually ignore all excited states, the depletion of the ground state, and the interaction between the active electron and the parent ion in the continuum. Furthermore, the

SAE approximation is usually applied. As such, all the electronic structure information is embedded in the highest occupied molecular orbital (HOMO) and the $I_p$. Even when other orbitals, such as HOMO-1, are considered, disentanglement of the orbitals is usually assumed and the active electron is approximated by plane waves [11, 22]. Such calculations can resolve the alignment angle dependent HHG signals and thus reveal the relation between the tomography of the HOMO and the HHG signal [11, 24, 25]. The limitation of these methods is that the role of correlated multielectron dynamics and ionic excited states are not fully considered. A quantum mechanical approach with all electrons included provides a more complete description of the process, although such a method requires extremely large scale computation.

A time dependent density functional theory (TDDFT) study of the HHG of $N_2$ was published in 2001 [26], in which the TDLB$_\alpha$ potential was adopted. This method treats the ground and excited states together with the continuum with sufficient accuracy. It also describes other strong field processes that accompany HHG, including ionization and excitation. The advantage of TDDFT is that it is in general less costly in terms of computation, while electron correlation is accounted for to some extent. In Figs. 12 and 13 of Ref. [26], a minimum is visible at 39 eV for both the 1064 nm and 800 nm fundamental wavelengths. The intensity applied there was $10^{14}$ W/cm$^2$. Here we will present more HHG data for a variety of laser intensities, frequencies, and molecular orientations to show that this relative stationary minimum is reproducible by our method.

A Cooper minimum is the mostly likely cause of a minimum that does not vary strongly with the molecular orientation angle. An important question, however, is: what makes the HOMO ($3\sigma_g$) atomic like? An earlier study of ours showed that the projection of outer region of the $3\sigma_g$ orbital is 82.7% $s$ and 17.1% $d_{z^2}$ [27]. This ratio varies with the radius $r$. Dipole matrix elements involving the $d_{z^2}$ orbital depend on the orientation. We therefore expect the dipole moment for recombination, which concerns the $p$ and $f$ scattering wave functions and their relative phases, to depend on the orientation.

Two-center interference [13] has also been discussed by Zimmermann *et al.* [28] and Gühr *et al.* [29]. Zimmermann *et al.* observed that the $3\sigma_g$ orbital of $N_2$ is a linear combination of $p$ and $s$ orbitals at the two atomic centers. For a destructive interference the free electron wave function as a plane wave should have a $2\pi$ phase shift between the two atomic centers for the $p$ component, whereas $\pi$ phase shift is needed for the $s$ component. Gühr *et al.*, on

the other hand, only considered a phase shift of $\pi$ between the atomic centers and found agreement between the interference model and the calculated HHG minimum using a SAE method for larger internuclear distances $R$ and the parallel orientation $\theta = 0$.

In this article we propose that resonance enhanced multiphoton excitation (REME) plays an important role in HHG spectra. Maxima occur at 23–26 eV for all orientations. Their positions overlap with the ionization potentials in photoelectron experiments [30], which correspond to excited ion states. We use time profile analysis to show that HHG peaks in this energy range have a large "multiphoton" component, which diminishes at the minimum. We postulate that this process is an excitation that results in an atomic-like orbital for the active electron. A significant contribution to HHG comes from recombination to Rydberg orbitals, which creates an isotropic Cooper Minimum. When this channel is considered, destructive two-center interference requires a $\pi$ phase difference for the plane wave between the two atomic centers and it overlaps with the Cooper Minimum for the parallel orientation.

We introduce the essential formalism of TDDFT in Sections II and III. In Section IV we show the calculated HHG spectra for various laser parameters and molecular orientations. We present time profile analysis and photoelectron experiment data that demonstrate the importance of excitation in creating HHG minima and maxima in Section V. The role of different molecular orbitals is analyzed in section VI. In Section VII we describe interference models that involve atomic like Rydberg orbitals. The conclusions are given in Section VIII.

## II. TIME DEPENDENT DENSITY FUNCTIONAL THEORY FOR MOLECULES IN STRONG FIELDS

A TDDFT method was developed for treating diatomic molecules interacting with a linearly polarized laser, whose polarization direction is parallel to the molecular axis [26, 31, 32]. Later this work was extended to treat arbitrary polarization directions for the study of the anisotropy of ionization and HHG [27, 33, 34]. We use the approach of Ref. [35], which includes multiple electronically excited states, the depletion of the ground state, and the interaction between the active electron and the parent ion in the continuum. We employ the $\mathrm{TDLB}_\alpha$ exchange-correlation functional, whose accuracy has been extensively benchmarked [26, 31, 34, 35]. Details of the method are given in previous articles [26, 31, 35]. The central theme of the TDDFT method that we implemented is a set of TD Kohn-Sham equations,

which are structurally similar to the TD Hartree-Fock equations, but include many-body effects through a local TD XC potential. We consider a quantum action integral [36–38]

$$A = \int_{t_0}^{t_1} dt \langle \Psi(t) | i\frac{\partial}{\partial t} - \hat{H}(t) | \Psi(t) \rangle, \tag{1}$$

where $\Psi(t)$ is the total $N$-electron wave function. When $\Psi(t)$ is represented by a single determinant,

$$\Psi(t) = \frac{1}{\sqrt{N!}} \det \left[ \psi_1(t) \psi_2(t) \cdots \psi_N(t) \right], \tag{2}$$

the total electron density at time $t$ is determined by the set of occupied single-electron orbital wave functions $\{\psi_{i\sigma}\}$ as

$$\rho(\boldsymbol{r}, t; R) = \sum_{\sigma} \sum_{i=1}^{N_\sigma} \rho_{i\sigma}(\boldsymbol{r}, t; R) = \sum_{\sigma} \sum_{i=1}^{N_\sigma} \psi_{i\sigma}^*(\boldsymbol{r}, t; R) \psi_{i\sigma}(\boldsymbol{r}, t; R), \tag{3}$$

where $i$ is the orbital index, $\sigma$ is the spin index, and $R$ is the internuclear distance. The spin orbital $\psi_{i\sigma}$ satisfies the one-electron Schrödinger-like equation, in atomic units,

$$\begin{aligned} i\frac{\partial}{\partial t}\psi_{i\sigma} &= \hat{H}(\boldsymbol{r}, t; R)\psi_{i\sigma} \\ &= \left[ -\frac{1}{2}\nabla^2 + v_{\text{nucl}}(\boldsymbol{r}; R) + \boldsymbol{E}(t) \cdot \boldsymbol{r} + \iiint d^3\boldsymbol{r}' \frac{\rho(\boldsymbol{r}', t; R)}{|\boldsymbol{r} - \boldsymbol{r}'|} + V_{\text{LB}_\alpha,\sigma}(\boldsymbol{r}, t; R) \right] \psi_{i\sigma}, \\ & \quad i = 1, 2, ..., N_\sigma, \end{aligned} \tag{4}$$

where $N_\sigma$ is the number of electrons that have $\sigma$ spin and $\boldsymbol{E}(t) = E(t)\hat{\boldsymbol{q}}$ is the electric field of the laser and $|\hat{\boldsymbol{q}}|$=1. The external potential due to the nuclear attraction is

$$v_{\text{nucl}} = -\frac{Z}{|\boldsymbol{R}_1 - \boldsymbol{r}|} - \frac{Z}{|\boldsymbol{R}_2 - \boldsymbol{r}|}, \tag{5}$$

where $\boldsymbol{R}_1$ and $\boldsymbol{R}_2$ are the coordinates of the two nuclei with charges $Z$. The TDLB$_\alpha$ potential is

$$\begin{aligned} V_{\text{LB}_\alpha,\sigma} &= \alpha v_{x\sigma}^{\text{LSDA}}(\boldsymbol{r}, t; R) + v_{c\sigma}^{\text{LSDA}}(\boldsymbol{r}, t; R) \\ & \quad - \frac{\beta x_\sigma^2(\boldsymbol{r}, t) \rho_\sigma^{\frac{1}{3}}(\boldsymbol{r}, t; R)}{1 + 3\beta x_\sigma(\boldsymbol{r}, t) \ln\{x_\sigma(\boldsymbol{r}, t; R) + [x_\sigma^2(\boldsymbol{r}, t; R) + 1]^{\frac{1}{2}}\}}, \end{aligned} \tag{6}$$

which contains two empirical parameters $\alpha$ and $\beta$. In Eq. (6), $v_{x\sigma}^{\text{LSDA}}$ and $v_{c\sigma}^{\text{LSDA}}$ are the local spin density approximation (LSDA) exchange and correlation potentials, which do *not* have the correct asymptotic behavior. The last term is the gradient correction with $x_\sigma(\boldsymbol{r}) = |\nabla \rho_\sigma(\boldsymbol{r})| / \rho_\sigma(\boldsymbol{r})^{4/3}$, which ensures the proper long-range asymptotic behavior $V_{\text{LB}_\alpha,\sigma} \to -1/r$ as $r \to \infty$.

## III. HHG POWER SPECTRUM CALCULATIONS

The numerical solution of the time-dependent equations is detailed in a recent publication [35]. Once the electron density $\rho(\boldsymbol{r}, t; R)$ is obtained, the induced dipole moment and dipole acceleration can be determined, respectively, as

$$d(R,t) = \iiint \rho(\boldsymbol{r}, t; R) q d^3\boldsymbol{r}, \tag{7}$$

where $q = \boldsymbol{r} \cdot \hat{\boldsymbol{q}}$ and

$$a(R,t) = \sum_\sigma \iiint \rho_\sigma(\boldsymbol{r}, t; R) \left[ -\frac{\partial v_{\rm nucl}(\boldsymbol{r}; R)}{\partial q} + E(t)\sin(\omega t) \right] d^3\boldsymbol{r}. \tag{8}$$

The HHG power spectrum is related to the Fourier transform of the respective time-dependent dipole moment or dipole acceleration:

$$d(R,\omega) \;=\; \frac{1}{t_f - t_i} \int_{t_i}^{t_f} d(R,t) e^{-i\omega t} dt, \tag{9}$$

$$a(R,\omega) \;=\; \frac{1}{t_f - t_i} \int_{t_i}^{t_f} a(R,t) e^{-i\omega t} dt = -\omega^2 d(R,\omega). \tag{10}$$

Finally, the spectral density (radiation energy per unit frequency range) is given by [33, 39]

$$S(R,\omega) = \frac{2}{3\pi c^3} \left| a(R,\omega) \right|^2 = \frac{2\omega^4}{3\pi c^3} \left| d(R,\omega) \right|^2, \tag{11}$$

where $c$ is the speed of light. We have checked that results obtained by calculating $a$ and $d$ are indistinguishable, which is an indication of numerical accuracy. Throughout the paper we plot $|d(R,\omega)|^2$ as the HHG power spectrum.

## IV. THE 39 EV MINIMUM AT THE EQUILIBRIUM INTERNUCLEAR DISTANCE

We consider a linearly polarized laser field with a $\sin^2$ pulse shape, 20 optical cycles in pulse length, and a laser intensity of $2{\times}10^{14}$ W/cm$^2$. The wavelength is 800 nm or 1064 nm. We fix $R$ at the equilibrium distance $R_e = 2.07\ a_0$. The $\alpha$ parameters of the TDLB$_\alpha$ potential for different $R$ values are listed in Ref. [27]. We show the HHG spectra in Fig. 1 for two laser frequencies. The electric field polarization is parallel to the molecular axis. This parallel orientation significantly reduces the size of the computation because the axial

symmetry is conserved. For both 800 nm and 1064 nm incident light, there is a minimum at 39 eV. Specifically, it is at the 25th harmonic for 800 nm and at the 33rd harmonic for 1064 nm, in agreement with experiments [16]. In Fig. 1 we also plot the spectrum for an 800 nm laser with an intensity of $1.5\times10^{14}$ W/cm$^2$. The minimum is more obvious with the lower laser intensity, which is consistent with experimental results [16]. The spectral density decreases from 30 eV to 39 eV is more abrupt for lower incidental laser intensity.

Experimentally measured positions of the discussed minimum for $N_2$ are not much influenced by the orientation angle ($\theta$) of the molecular axis relative to the polarization direction of the laser field. This is a major difference between the minimum for $N_2$ and those for $CO_2$.

In Fig. 2 we plot the HHG spectrum for three values of $\theta$. The laser intensity is $2 \times 10^{14}$ W/cm$^2$ and the wavelength is 800 nm. The HHG intensity decreases from the parallel orientation to $\theta = 45^\circ$, and further to the perpendicular orientation for most harmonics, which is consistent with experimental observations. For all three orientations there is a minimum at 39 eV, also in agreement with experiment [40].

Earlier work on $H_2$ showed that HHG spectra calculated at the equilibrium distance differ considerably from HHG spectra calculated with molecular vibration taken into account [41]. The reason is that for $H_2$ the vertical $I_p(R)$ varies significantly over $R$, which causes the phase $\phi(\omega, R)$ of HHG to oscillate over $R$ as well. In Fig. 3 we plot the ground state vibrational wave function $\chi_0(R)$ of $N_2$ together with $I_p(R)$. This $I_p(R)$ is much flatter than that for $H_2$ in the region where the nuclear wave function has significant amplitude.

If we express $|D(\omega, \nu = 0)|^2$, in which $\nu$ is the vibrational quantum number, as

$$|D(\omega, \nu = 0)|^2 = |\langle\chi_0(R)|d(R, \omega)e^{i\phi(\omega,R)}|\chi_0(R)\rangle|^2, \tag{12}$$

we see that a large phase variation causes cancellation in Eq. (12) and makes $|D(\omega, 0)|^2$ very different from $|d(\omega, R_e)|^2$. Due to the importance of the $R-$dependent phase, Eq. (12) can be approximated by

$$|D(\omega, \nu = 0)|^2 \approx \left|\langle\chi_0|e^{-iI_p(R)\tau(\omega)}|\chi_0\rangle\right|^2 |d(\omega, R_e)|^2, \tag{13}$$

where $\tau$ is the recombination time defined in the strong field approximation (SFA). It was shown that this "SFA phase" formula reproduces the measured $D_2$ to $H_2$ HHG ratio [41].

It is much less costly to evaluate Eq. (13) than to evaluate Eq. (12), because Eq.(12) involves repeatedly solving TDDFT equations for different $R$ values. In recent work on $H_2$,

the error caused by using the SFA phase formula is estimated to be within 7 % for similar laser parameters [41]. We expect the error in the case of $N_2$ to be even smaller, because $|d(R,\omega)|$ is more flat as a function of $R$ for $N_2$ than for $H_2$ due to the flatter $I_p(R)$ of $N_2$.

As a measure of the effect of the zero point vibration in $N_2$, we calculate the ratio $|D(\omega,\nu=0)|^2/|d(\omega,R_e)|^2$. When using Eq. (13) this ratio becomes $\left|\langle\chi_0|e^{-iI_p(R)\tau(\omega)}|\chi_0\rangle\right|^2$ and it is always less than 1 because only the phase $\phi$ is considered as a function of $R$ in Eq. (13). In Fig. 4 we plot the ratio of the HHG intensity calculated with Eq. (13) as a function of $\omega$ for $R=R_e$. This ratio at the discussed minimum is 0.98 for the 1064 nm laser and 0.97 for the 800 nm laser, and it remains close to 1 at other harmonics. This justifies our approximation of $|d(\omega)|^2 \equiv |d(\omega,R_e)|^2 \approx |D(\omega,\nu=0)|^2$ for $N_2$ throughout this paper.

## V. REME AND ITS ROLE IN HHG MAXIMA AND MINIMA

A maximum appears around 23–26 eV for the 800 nm laser and at similar energies for the 1064 nm laser but with more structure. Compared to the HHG intensity at the ionization threshold, the maximum is more enhanced than what we expect from constructive interference. We further observe that photon energies of the maxima overlap with $I_p$s measured in photoelectron experiments. In Table I we list the lowest eight doublet $N_2^+$ states observed in the photoelectron experiment [30]. The vertical $I_p$ of $N_2$ at $R=R_e$ for each state is obtained from experiment, from multireference configuration interaction (MRCI) [42], and from DFT calculations. For each state we also tabulate the dominant excitation with respect to the $X\,^2\Sigma_g^+$ ground state of the ion. In the DFT calculation, we use the $LB_\alpha$ potential with exactly the same $\alpha$ coefficient as in our TD calculations. The orbital energies ($\epsilon$) of $N_2$ are listed in Table II. The vertical $I_p$ from the ground state of $N_2$ to the $X\,^2\Sigma_g^+$ state of the ion is calculated as the negative of the orbital energy of the $3\sigma_g$ HOMO. For other ionic states, the orbital energy differences for orbitals involved in the dominant excitation of the ion are added. For example, the $I_p$ from the ground state of $N_2$ to the $D\,^2\Pi_g$ state of the ion is calculated as $I_p = -\epsilon_{3\sigma_g} + \epsilon_{3\sigma_g} + \epsilon_{1\pi_g} - 2\epsilon_{1\pi_u} = \epsilon_{1\pi_g} - 2\epsilon_{1\pi_u}$.

With the laser polarization parallel to the molecular axis, allowed transitions from the $X\,^2\Sigma_g^+$ ground state are limited to the $B\,^2\Sigma_u^+$ and $C\,^2\Sigma_u^+$ states in Table I with odd numbers of photons, or to the $F\,^2\Sigma_g^+$ state with even number of photons. From intermediate output and analysis of our TDDFT formalism, we identify contributions of these excited states to

HHG. First we rewrite $\Psi(t)$ [Eq. (2)] as

$$\tilde{\Psi}(t) = \sum_{ll'} b_{ll'}(t)\Theta_l^{\rm ion}\varphi_{l'}^{\rm elec}, \tag{14}$$

where $\Theta_l^{\rm ion}$ is an orbital product corresponding to a field-free ionic configuration and $\varphi_{l'}^{\rm elec}$ is a one electron function. We do not use determinants since that is not necessary for computing the dipole moment. The ion and electron are treated together in our calculation and an absorbing boundary is placed at 40 $a_0$ radius to simulate ionization. The summation includes the ground state, excited states, and continuum states. The Fourier transform of the dipole becomes

$$\begin{aligned} d(\omega) &= \frac{1}{t_f - t_i}\int_{t_i}^{t_f} \sum_{l_1 l_2 l_3 l_4} b^*_{l_1 l_2}(t)\langle\Theta_{l_1}^{\rm ion}\varphi_{l_2}^{\rm elec}|\hat{d}|\Theta_{l_3}^{\rm ion}\varphi_{l_4}^{\rm elec}\rangle b_{l_3 l_4}(t)e^{-i\omega t}dt \\ &= \sum_{l_1 l_3}\langle\Theta_{l_1}^{\rm ion}|\hat{d}|\Theta_{l_3}^{\rm ion}\rangle\frac{1}{t_f - f_i}\int_{t_i}^{t_f}\sum_{l_2} b^*_{l_1 l_2}(t)b_{l_3 l_2}(t)e^{-i\omega t}dt + \\ &\quad \sum_{l_2 l_4}\langle\varphi_{l_2}^{\rm elec}|\hat{d}|\varphi_{l_4}^{\rm elec}\rangle\frac{1}{t_f - f_i}\int_{t_i}^{t_f}\sum_{l_1} b^*_{l_1 l_2}(t)b_{l_1 l_4}(t)e^{-i\omega t}dt \end{aligned} \tag{15}$$

where $\hat{d}$ is the dipole operator and we used the orthonormality of the orbitals. In situations where the only contribution comes from recombination, at time $\tau(\omega)$, from a free electron state with energy $\epsilon_k = \frac{\hbar^2 k^2}{2m_e}$ to the ground state with energy $-I_p$ and the ion remains in the ground state, this model reduces to the SFA formalism with $d(\omega) \propto \langle\varphi_{3\sigma_g}^{\rm elec}|\hat{d}|\varphi_{\boldsymbol{k}}^{\rm elec}\rangle$ and

$$\hbar\omega = \epsilon_k - (-I_p) = \frac{\hbar^2 k^2}{2m_e} + I_p. \tag{16}$$

In our calculations, however, resonances couple the ground state to excited states of the ion and the active electron. We evaluate Eqs. (7) and (9) with $\rho(t)$ obtained by solving the TDDFT equations. For the purpose of analysis, we evaluate the Fourier components of $b_{ll'}(t)$,

$$b_{ll'}(\omega) = \int_{t_i}^{t_f}\langle\Theta_l^{\rm ion}\varphi_{l'}^{\rm elec}|\tilde{\Psi}(t)\rangle e^{-i\omega t}dt. \tag{17}$$

The field free wave functions $\Theta_l^{\rm ion}$ and $\varphi_{l'}^{\rm elec}$ are from DFT calculations on the same spatial grid and $\tilde{\Psi}(t)$ is obtained in our TDDFT calculations. Contributions to $d(\omega)$ [Eq. 15] arise from products $b_{l_1 l_2}(\omega_0)b_{l_3 l_4}(\omega_1)$ whenever $\omega = \omega_1 - \omega_0$. Since depletion of the ground state is small, the main contribution arises from $\hbar\omega_0 = -I_p$ and, for an harmonic with photon energy $\hbar\omega$, we have $\hbar\omega_1 = \hbar\omega - I_p$. Among $\sim$ 10,000 coefficients $b_{ll'}(-I_p/\hbar)$ and

$b_{ll'}(\omega - I_p/\hbar)$, we select the largest ones. For $b_{ll'}(-I_p/\hbar)$, apart from the ground state contribution $X\,^2\Sigma_g^+\,3\sigma_g$, we also found significant contribution from $(C\,^2\Sigma_u^+)\,3\sigma_u$ because of the resonance. For $b_{ll'}(\omega - I_p/\hbar)$, the contribution from $(X\,^2\Sigma_g^+)\varphi_{\boldsymbol{k}'}$, with $\hbar\omega - I_p = \epsilon_{k'}$, where $\epsilon_{k'}$ is the energy of the electron in the continuum, is negligible. The largest contribution is from $(C\,^2\Sigma_u^+)(\varphi_{\boldsymbol{k}} + b\,3\sigma_g)$, where $b$ is a constant, $\hbar\omega - I_p = \epsilon_k + \Delta E_{\rm exc}^{\rm ion}$, and $\Delta E_{\rm exc}^{\rm ion} = E(C\,^2\Sigma_u^+) - E(X\,^2\Sigma_g^+)$ is the excitation energy of the ion. Therefore we have

$$\hbar\omega = I_p + \epsilon_k + \Delta E_{\rm exc}^{\rm ion}. \tag{18}$$

The dipole according to Eq. (15) is

$$d(\omega) \propto A\langle X\,^2\Sigma_g^+|\hat{d}|C\,^2\Sigma_u^+\rangle + B\langle 3\sigma_u|\hat{d}|\varphi_{\boldsymbol{k}'}\rangle, \tag{19}$$

where constants $A$ and $B$ are significantly larger than those of other contributions.

Excitation of the ion from the $X\,^2\Sigma_g^+$ to the $C\,^2\Sigma_u^+$ state and excitation of the electron from $3\sigma_g$ to $3\sigma_u$ are important. In neutral $N_2$ orbital excitation from $3\sigma_g$ to $3\sigma_u$ produces the $c_4'\,^1\Sigma_u^+$ Rydberg state. We extract the following mechanism accordingly for H15 and up to the 39 eV minimum.

$$N_2\ (X\,^1\Sigma_g^+) + 9h\nu \quad \overset{\text{excitation}}{\longrightarrow} \quad N_2\ (c_4'\,^1\Sigma_u^+) \tag{20}$$

$$N_2\ (c_4'\,^1\Sigma_u^+) + 6h\nu \quad \overset{\text{ionization}}{\longrightarrow} \quad N_2^+\ (C\,^2\Sigma_u^+) + e^-, \tag{21}$$

$$e^- + nh\nu \quad \overset{\text{acceleration}}{\longrightarrow} \quad e^{-*}, \quad n = 1, ..., 10, \tag{22}$$

$$N_2^+\ (C\,^2\Sigma_u^+) + e^{-*} \quad \overset{\text{recombination}}{\longrightarrow} \quad N_2\ (c_4'\,^1\Sigma_u^+) + h\nu' \quad [\nu' = (6+n)\nu]. \tag{23}$$

In this "four step" mechanism, excitation is added prior to the three steps of HHG and the product of the ionization is an ion in an excited state, rather than in the ground state. The excitation and ionization steps are enhanced by multiphoton resonance. The recombination step consists of two single-electron processes of ion de-excitation $C\,^2\Sigma_u^+ \to X\,^2\Sigma_g^+$ and the high electron goes from the continuum with energy $\epsilon_k$ to the $3\sigma_u$ orbital. The combination of the $X\,^2\Sigma_g^+$ ionic state and $3\sigma_u$ electronic orbital gives the $c_4'\,^1\Sigma_u^+$ state of $N_2$.

The time profile of $|d_\omega(t)|$ obtained by the wavelet expansion [31] distinguishes a three step process from a multiphoton process for HHG with photon energy $\hbar\omega$. An example of the "three step" process is H25 (the minimum at 39 eV) at $R_e$ in Fig. 5. It exhibits two "recombination" peaks per optical cycle and twice per cycle $|d_{25\omega_0}(t)|$ drops to zero. An

example of a pure multiphoton process is H9 (slightly below the $I_p$), because its energy is too low for tunneling ionization. Its time profile in Fig. 5 shows no periodicity and it correlates with the laser intensity. For H11 (17 eV, slightly above the vertical $I_p$), although the periodic recombination peaks are visible, the dominant contribution is still the multiphoton process, enhanced by the multiphoton resonance with highly excited states and virtual states near the ionization threshold. As a result, $|d_{11\omega_0}(t)|$ does not drop to zero between two peaks, as in the case when the three step process is dominant. Harmonic H15, the 23 eV maximum, has a similar profile. The contribution from the multiphoton resonance matches that of H9, and is significantly larger than that of H11. The contribution of multiphoton resonance decreases with increasing harmonic order and drops to near zero for H25, the weak minimum, and for higher harmonics. We observe similar patterns in time profiles for $\theta = 45°$ and $\theta = 90°$.

Mechanisms outlined in Eqs. (20)-(23) are consistent with significant multiphoton contributions for harmonics between the maximum and minimum, which cannot be explained by interference models that only consider the three-step mechanism. In these "four step" mechanisms we propose, multiphoton contributions arise from the excitation and ionization steps, they are reflected in the first term of Eq. (19), and they are enhanced by the resonances listed in Table I. Compared to the three step mechanism, the additional excitation step makes the free electron recombine to a higher orbital than the HOMO, as in the second term of Eq. (19), which bears a significance in interferences that create HHG minima.

The anisotropy of the calculated HHG intensities, defined as the ratio between $|d(\omega)|^2$ for $\theta = 0°$ and for $\theta = 90°$, supports our interpretation that excitation causes HHG maxima at all orientations. The anisotropy increases with the harmonic order $n$, from $n = 1$ to $n = 7$, which occurs at 11 eV. Then it reduces for $n = 9$ and $n = 11$, possibly due to the $X\,^2\Sigma_g^+$–$A\,^2\Pi_u$ resonance for the perpendicular orientation (see Table I). Then it increases for $n = 13$ and $n = 15$, which is the 23 eV maximum for the parallel orientation. The anisotropy maximizes here. This is consistent with the selection rule that prohibits the $X\,^2\Sigma_g^+$–$C\,^2\Sigma_u^+$ multiphoton transition for the perpendicular orientation. For $n = 17$ (at 26 eV), the anisotropy has a minimum, which is due to the $X\,^2\Sigma_g^+$–$2\,^2\Pi_u$ resonance prohibited for the parallel orientation but allowed for other orientations (Table I). From 26 to 36 eV, the anisotropy appears constant. For the perpendicular orientation, the peaks for $n = 25$, 27, and 29 (at 39–45 eV) have the shape of a short plateau before the cutoff. For the perpendicular orientation, we propose the following mechanism for H17 and up to the

39 eV minimum.

$$N_2\ (X\,^1\Sigma_g^+) + 9h\nu \quad \overset{\text{excitation}}{\longrightarrow} \quad N_2\ (c_3\,^1\Pi_u), \tag{24}$$

$$N_2\ (c_3\,^1\Pi_u) + 8h\nu \quad \overset{\text{ionization}}{\longrightarrow} \quad N_2^+\ (2\,^2\Pi_u) + e^-, \tag{25}$$

$$e^- + nh\nu \quad \overset{\text{acceleration}}{\longrightarrow} \quad e^{-*}, \quad n = 1, ..., 8, \tag{26}$$

$$N_2^+\ (2\,^2\Pi_u) + e^{-*} \quad \overset{\text{recombination}}{\longrightarrow} \quad N_2\ (c_3\,^1\Pi_u) + h\nu'$$

$$[\nu' = (8+n)\nu]. \tag{27}$$

The $c_3\,^1\Pi_u$ state of $N_2$ corresponds to an ion in the $X\,^2\Sigma_g^+$ state and the electron in the $2\pi_u$ orbital. The dipole matrix element analogous to Eq. (19) for the perpendicular orientation is

$$d(\omega) \propto C\langle X\,^2\Sigma_g^+|\hat{d}|2\,^2\Pi_u\rangle + D\langle 2\pi_u|\hat{d}|\varphi_{\boldsymbol{k}}\rangle, \tag{28}$$

where $C$ and $D$ are constants.

The $X\,^2\Sigma_g^+$–$2\,^2\Pi_u$ and $X\,^2\Sigma_g^+$–$C\,^2\Sigma_u^+$ resonances, which create maxima for the perpendicular and parallel orientations, respectively, are both allowed for the $\theta = 45°$ orientation. The four step mechanisms that we propose [Eqs. (20)-(27)] for perpendicular and parallel orientations therefore both apply here and at any other orientations in between the parallel and the perpendicular. In addition the $X\,^2\Sigma_g^+ \rightarrow {}^2\Pi_g$ transitions are forbidden for both the parallel and the perpendicular orientation, but allowed for $\theta = 45°$. As such the HHG intensity at $\theta = 45°$ orientation is much closer to that for the parallel orientation than that for the perpendicular orientation. Figure 2 shows a near constant ratio between the HHG intensity of the parallel and $\theta = 45°$ orientation for most of the harmonics.

In experiments aligned molecules contain a distribution of orientations. Calculated HHG spectra for the above three typical angles show that a 23–26 eV maximum due to multiphoton excitations of the ion exists for all orientations, despite the different selection rules that apply to parallel and perpendicular orientations. From these maxima, the HHG intensity decreases to the same 39 eV minimum for all orientations.

## VI. CONTRIBUTION OF MOLECULAR ORBITALS

Molecular orbitals have been an important concept in strong field theories. Here we discuss orbital assignments to the four steps. For the parallel orientation the excitation step consists of orbital transition $3\sigma_g \rightarrow 3\sigma_u(2p\sigma_u)$. Ion excitation $1\pi_u \rightarrow 1\pi_g$ occurs in the

ionization step. For the perpendicular orientation, $3\sigma_g \rightarrow 2\pi_u(3p\pi_u)$ occurs in the excitation step and $2\sigma_u \rightarrow 1\pi_g$ in the ionization step. For orientations in between, a combination of these orbitals and transitions occurs. Orbital energies are listed in Table II. Our assignment of the second step consists of the ionization of the highest electron from the $3\sigma_u$ or $2\pi_u$ orbital while exciting a second electron. Assignments of excitations are listed in Table I. Finally the electron returns to the $3\sigma_u$ or $2\pi_u$ orbital and the ion returns to the ground state upon recollision.

We consider two-electron processes for the ionization steps important for creating the 23–26 eV maxima, which we interpret as a multiphoton resonance with the excited ionic state. In order to support this model, we investigate contributions of individual initially occupied orbitals, when coupling between orbitals is removed. In our TDDFT calculation, all orbitals are coupled through the Coulomb and XC terms in Eq. (2). The coupling becomes negligible when we artificially shift the orbital energies of all but one occupied orbital down by 1.5 $E_h$ (40.8 eV). The unoccupied orbitals are not shifted. The electron density for the orbitals with shifted energies becomes frozen to the initial distribution obtained from field free DFT calculations. As such only the unshifted orbital contributes to the dipole, i.e., $|d(\omega)|^2 \approx |d_j(\omega)|^2$, in which $j$ is index for the unshifted orbital.

In Fig. 6, we plot calculated contributions from the $3\sigma_g$ (HOMO), $1\pi_u$ (HOMO-1), and $2\sigma_u$ (HOMO-2) orbitals to the HHG of $N_2$ for a 800 nm laser of $2 \times 10^{14}$ W/cm$^2$ with the molecule parallel to the polarization direction of the field. These contributions are obtained by three different calculations in which we freeze electrons in turn in all but one contributing orbital using the method described above. The contribution of the HOMO is dominant. In this orientation the contribution of the $2\sigma_u$ orbital is larger than that of the $1\pi_u$ orbital for most harmonics, in spite of its lower energy.

The 39 eV minimum appears in the contribution from $3\sigma_g$. From 17 to 30 eV, there is a high plateau for $3\sigma_g$, and the 39 eV minimum is at the beginning of a second plateau. We also find the $\sim$39 eV minimum in the $3\sigma_g$-only calculation for other orientations. Time-profile analysis for these $3\sigma_g$-only calculations show that the excitation step [Eq. (20)] is still there. In this case, instead of Eq. (19) the recombination dipole matrix element becomes $d(\omega) \propto A'\langle 3\sigma_g|\hat{d}|2\sigma_u\rangle + B'\langle 3\sigma_u|\hat{d}|\varphi_{\mathbf{k}}\rangle$. With only the two $3\sigma_g$ electrons are considered, the mechanism remains very similar to those in Eqs. (20)-(23). The excitation step involves the $3\sigma_g$ to $3\sigma_u$ transition, the other $3\sigma_g$ electron ionizes in the next step and accelerates in

the field before recombines to the $3\sigma_u$ orbital while the other electron goes back to the $3\sigma_g$ orbital.

The largest difference between the $3\sigma_g$-only contribution shown in Fig. 6 and the all-electron results in Fig. 1 concerns the maximum at ∼23.3 eV (H15). According to the all electron calculation, the ratio between this maximum and the minimum at 17 eV is 8, whereas the same ratio from the $3\sigma_g$-only calculation is only 2. It demonstrates significant contribution from other orbitals to the maximum.

We propose that the most important contribution to the maximum comes from the transition between the $1\pi_u$ and $1\pi_g$ orbitals, which is consistent with intermediate output and our model in which the ionization step is a two-electron process. To show effects of two-electron processes in which the highest electron ionizes while a second electron is excited from the $1\pi_u$ to the $1\pi_g$ orbital, we shift the energy of the unoccupied $1\pi_g$ orbital up by 0.25 $E_h$ (6.8 eV) in an all-electron calculation. The HHG spectrum calculated this way is plotted in Fig. 7 as the red solid line and it is shifted slightly to the right to compare it with the unshifted spectrum. The 23.3 eV maximum is reduced 8-fold. The intensity of emissions at 33 and 36 eV increases. The HOMO is a $\sigma$ orbital, which is not coupled to $\pi$ orbitals by the laser field when $\theta = 0°$. This shows that it has to be a two-electron process that involves another electron initially in the $1\pi_u$ orbital that creates the 23.3 eV maximum. A TDDFT method may not treat two or many electron excitations very accurately. Resolving harmonic orders, on the other hand, does not require high accuracy. For the 800 nm laser field, for instance, the energy difference between two adjacent odd harmonics is as large as 3.10 eV.

## VII. INTERFERENCE MODELS INVOLVING RYDBERG STATES FOR EXPLAINING THE MINIMUM

A HHG minimum occurs when the contribution shown in Eq. (19) or the analogous dipole matrix element for other orientations becomes minimized. The excitation step shown in Eqs. (20) and (24) creates Rydberg molecules when $N_2$ is exposed to an intense 800 nm linearly polarized laser. The Rydberg state is $c_4' \, ^1\Sigma_u^+$ for the parallel orientation, $c_3 \, ^2\Pi_u$ for the perpendicular orientation, and a linear combination of them for other orientations. Both Rydberg states have principle quantum number $n = 3$, converge to the ground state

of the ion, and their energies are very similar: $c_4' \, ^1\Sigma_u^+$ is 12.93 eV above the ground state while $c_3 \, ^2\Pi_u$ is at 12.91 eV [43, 44]. Highest orbitals for both the parallel and perpendicular orientations, $3\sigma_u$ ($2p\sigma_u$) and $2\pi_u$ ($3p\pi_u$) orbitals, are highly atomic-like and have more than 99.8% $p$ character. Their orbital energies are very similar (Table II) as well. As a result, the dipole matrix elements involving these $p$ Rydberg orbitals create minima analogous to the Cooper minimum in Ar associated with the $3p$ orbital. At energies ($k$ values) where $\langle 3\sigma_u|\hat{d}|\varphi_{\mathbf{k}}\rangle$ in Eq. (19) becomes minimized, $\langle X \, ^2\Sigma_g^+|\hat{d}|C \, ^2\Sigma_u^+\rangle$ is also significantly reduced, because the mixing between $\varphi_{\mathbf{k}}$ and $3\sigma_g$, which leads to $\langle X \, ^2\Sigma_g^+|\hat{d}|C \, ^2\Sigma_u^+\rangle$ disappears as well when $3\sigma_u$ and $\varphi_{\mathbf{k}}$ no longer couples.

Cooper minima of Rydberg molecules created in resonance enhanced multiphoton ionization photoelectron spectra have been studied theoretically for NO [45]. It was shown that the minima have much lower energy and the energy variation with respect to the orientation angle is within 3 eV. We expect similarities for the HHG of $N_2$ with 800 nm intense lasers: recombination matrix element involving the Rydberg state have a lower energy than 39 eV and the excitation energy makes up the difference. The orientation dependence is very small.

At any orientation other than the perpendicular, the Rydberg orbital involved in HHG resembles a $4p$ atomic orbital, with one radial node at $\sim R/2$ and another at $\sim 2$ $a_0$. The Rydberg orbital at the perpendicular orientation has one radial node remaining at $\sim 2$ $a_0$, while the other node tends to the plane that goes through the origin. At the parallel orientation in particular, one radial node goes through the two atomic centers, we therefore expect the Cooper minimum, which is due to the nodal structure, to coincide with the two-center interference minimum at the parallel orientation. At other orientations the Cooper minimum remains at similar photon energies, because the change in radial nodes are very subtle as the orientation is varied. The two-center interference, however, depends on the distance between two planes, $R\cos\theta$, and its minimum becomes unnoticeable when $\theta$ is large, because it is either at the low intensity plateau beyond the Cooper minimum or even beyond the cutoff energy.

Here we use a modified two-center interference model at the parallel orientation to further demonstrate the important influence of excitation on the minimum. With the REME and Rydberg orbital considered, we propose a model that has two major differences compared to earlier work by Lein *et al.* [13] and by Zimmermann *et al.* [28]. (i) Since we identify the Rydberg orbital ($2p\sigma_u$) rather than the HOMO ($2p\sigma_g$) as the molecular orbital for

recombination, the destructive interference requires the free-electron plane wave to have a $\pi$ phase difference between the atomic centers, rather than a difference of $2\pi$, i.e.

$$|\mathbf{k}|R\cos\theta = \pi, \tag{29}$$

where $\mathbf{k}$ is the wave vector of the free electron and $\theta$ is the angle between the molecular axis and the polarization direction of the electric field of the laser. (ii) When a multiphoton resonance with an excited state makes a significant contribution, the photon energy of the high harmonic is given by Eq. (18). As is often done in the SFA [13], we compute the wave number $k = |\boldsymbol{k}|$ from

$$\frac{\hbar^2 k^2}{2m_e} = \epsilon_k + I_p, \tag{30}$$

because the free electron has a higher kinetic energy near the atomic centers. The photon energy given by Eq. (18) becomes

$$\hbar\omega = \frac{\hbar^2 k^2}{2m_e} + \Delta E_{\rm exc}^{\rm ion}. \tag{31}$$

In our TDDFT calculation for $\theta = 0^\circ$, excitations that create the HHG maximum are dominated by the $1\pi_u \leftrightarrow 1\pi_g$ orbital transition. We therefore approximate

$$\Delta E_{\rm exc}^{\rm ion} = \epsilon_{1\pi_g}(R) - \epsilon_{1\pi_u}(R) \equiv \Delta\epsilon(R), \tag{32}$$

where $\epsilon_i$ is the orbital energy of orbital $i$. At the equilibrium internuclear distance, $\epsilon_{1\pi_g}(R_e) - \epsilon_{1\pi_u}(R_e)$ is approximately 6 photons' energy for 800 nm lasers, consistent with Eq. (23). In order for the destructive interference between the two atomic centers to occur, $|\mathbf{k}|$ has to satisfy Eq. (29). Thus for $\theta = 0^\circ$ we predict the HHG minimum at

$$\hbar\omega_{min} \;=\; \frac{\hbar^2\pi^2}{2m_e R^2} + \Delta\epsilon(R). \tag{33}$$

We calculate a series of HHG spectra for $1.9 \le R \le 2.7$ $a_0$ using the TDDFT method. Results are shown in Fig. 8. For $R$ = 2.7, 2.6, and 2.5 $a_0$, the minimum is in between two maxima. For $R$ = 2.3, 2.2, 2.1, 2.0, and 1.9 $a_0$, the shape above the minimum is more like a plateau rather than a maximum. Note that $R$ = 2.1 $a_0$ is very close to the $N_2$ equilibrium distance ($R_e$ = 2.07 $a_0$). In Fig. 8 we use vertical red lines to mark $\hbar\omega_{min}$ predicted by Eq. (33). They agree with the minimum according to the TDDFT calculation for $R \ge 1.9$ $a_0$. For $R$ = 1.5 and 1.6 $a_0$, the minimum according to the modified two-center interference model is larger than the cutoff energy, therefore the model is no longer

applicable. Considering that the HHG peaks calculated by TDDFT are odd harmonics of the principle frequency, whereas $\hbar\omega_{min}$ calculated by Eq. (33) are not limited to be harmonics, the agreement between the two methods is remarkable.

In Table III we list $\hbar\omega_{min}$ predicted without considering the excitation, i.e.,

$$\hbar\omega_{min} = \frac{\hbar^2\pi^2}{2m_e R^2} \tag{34}$$

and using Eq. (33) for the series of $R$ values used in Fig. 8. The difference between the two methods is $\Delta\epsilon(R)$ estimated by Eq. (32). It varies from 4.5 eV for $R = 2.7\ a_0$ to 11.6 eV for $R = 1.9\ a_0$, which offers a crucial modification of the two-center interference model. If we do not include the excitation energy and do not consider the symmetry of the Rydberg orbital, but use the symmetry of the HOMO instead, positions of the minimum would be four times of the values predicted by using Eq. (34), different from the TDDFT results by a large extent.

The agreement between this model, which considers both the Rydberg orbital and the excitation energy, and the TDDFT results offers further support of our four step model. It demonstrates the importance of the multiphoton excitation in the shape of the HHG spectra calculated by the TDDFT calculation.

## VIII. DISCUSSION AND CONCLUSIONS

We calculate HHG spectra of $N_2$ using a TDDFT method that has been extensively benchmarked. The influence of the laser intensity and wavelength is analyzed as well as the effect of molecular vibration and orientation. A minimum appears at 39 eV in all of our results for the equilibrium geometry regardless of laser parameters and molecular orientation, in agreement with experiments. Molecular vibration does not play a significant role in the HHG because the vertical $I_p$ of $N_2$ is relatively flat in the region sampled by the ground state vibrational wave function.

Calculated spectra exhibit maxima at 23–26 eV depending on laser parameters and the molecular orientation. We propose that REME causes the maxima. This interpretation is supported by the following: (i) Photon energies of maxima are in resonance with excited states of $N_2$ and their orientation dependence is consistent with the selection rules. (ii) The time profiles of maxima show significant contribution of multiphoton processes, they do not drop to zero twice per optical cycle as in the case of a typical three-step HHG

process. Considering that photon energies of maxima are much higher than the ionization threshold, the only explanation for a multiphoton process is multiphoton excitation enhanced by resonance. (iii) Shifting the energy of an unoccupied $\pi$-orbital causes significant changes in the harmonic of the maximum when the molecular axis is parallel to the polarization of the field. This confirms our assignment of excited states involved in the resonance.

We propose a four step model for the HHG between the maxima and the ∼39 eV minima, which includes excitation, ionization, acceleration, and recombination steps. This mechanism is based on analysis of our TDDFT formalism and supported by intermediate output, time profile analysis, orbital contribution analysis, and our assignment for the HHG maxima. The excitation step results in a Rydberg state, which is atomic like. The Rydberg orbital is a combination of the $3\sigma_u$ and $2\pi_u$ orbitals depending on the molecular orientation. Regardless of the orientation, however, the orbital has more than 99.8% of $p$ atomic orbital character, which gives rise to a Cooper like minimum that is invariant to orientation. A radial node is at $\sim R/2$ radius, going through two atomic centers for the parallel orientation. For the parallel orientation only, the Cooper minimum coincides with the minimum predicted by a two-center interference model, in which we consider the symmetry of the Rydberg orbital and the excitation energy. Minima predicted by this modified two-center interference model agree with TDDFT calculations with a series of $R$ values, which offers more support of the four step model that involves Rydberg orbitals and excited ionic states.

**Acknowledgments**

This work is supported by the National Science Foundation Award No. PHY-0855676.

[1] A. McPherson, G. Gibson, H. Jara, U. Johann, T. S. Luk, I. A. McIntyre, K. Boyer, and C. K. Rhodes, J. Opt. Soc. Am. B **4**, 595 (1987).

[2] X. F. Li, A. L'Huillier, M. Ferray, L. A. Lompré, and G. Mainfray, Phys. Rev. A **39**, 5751 (1989).

[3] N. L. Wagner, A. Wüest, I. P. Christov, T. Popmintchev, X. Zhou, M. M. Murnane, and H. C. Kapteyn, Proc. Natl. Acad. Sci. USA **103**, 13279 (2006).

[4] S. Baker, J. S. Robinson, C. A. Haworth, H. Teng, R. A. Smith, C. C. Chirilă, M. Lein, J. W. G. Tisch, and J. P. Marangos, Science **312**, 424 (2006).

[5] S. Baker, J. S. Robinson, M. Lein, C. C. Chirilă, R. Torres, H. C. Bandulet, D. Comtois, J. C. Kieffer, D. M. Villeneuve, J. W. G. Tisch, et al., Phys. Rev. Lett. **101**, 053901 (2008).

[6] W. Li, X. Zhou, R. Lock, S. Patchkovskii, A. Stolow, H. C. Kapteyn, and M. M. Murnane, Science **322**, 1207 (2008).

[7] H. J. Wörner, J. B. Bertrand, D. V. Kartashov, P. B. Corkum, and D. M. Villeneuve, Nature **466**, 604 (2010).

[8] D. Shafir, H. Soifer, B. D. Bruner, M. Dagan, Y. Mairesse, S. Patchkovskii, M. Y. Ivanov, O. Smirnova, and N. Dudovich, Nature **485**, 343 (2012).

[9] J. B. Bertrand, H. J. Wörner, P. Hockett, D. M. Villeneuve, and P. B. Corkum, Phys. Rev. Lett. **109**, 143001 (2012).

[10] O. Smirnova, Y. Mairesse, S. Patchkovskii, N. Dudovich, D. Villeneuve, P. Corkum, and M. Y. Ivanov, Nature **460**, 972 (2009).

[11] S. Haessler, J. Caillat, W. Boutu, C. Giovanetti-Teixeira, T. Ruchon, T. Auguste, Z. Diveki, P. Breger, A. Maquet, B. Carré, et al., Nat. Phys. **6**, 200 (2010).

[12] A. E. Boguslavskiy, J. Mikosch, A. Gijsbertsen, M. Spanner, S. Patchkovskii, N. Gador, M. J. Vrakking, and A. Stolow, Science **335**, 1336 (2012).

[13] M. Lein, N. Hey, R. Velotta, J. P. Marangos, and P. L. Knight, Phys. Rev. A **66**, 023805 (2002).

[14] J. W. Cooper, Phys. Rev. **128**, 681 (1962).

[15] W. Boutu, S. Haessler, H. Merdji, P. Breger, G. Waters, M. Stankiewicz, L. J. Frasinski, R. Taieb, J. Caillat, A. Maquet, et al., Nat. Phys. **4**, 545 (2008).

[16] H. J. Wörner, J. B. Bertrand, P. Hockett, P. B. Corkum, and D. M. Villeneuve, Phys. Rev. Lett. **104**, 233904 (2010).

[17] H. J. Wörner, H. Niikura, J. B. Bertrand, P. B. Corkum, and D. M. Villeneuve, Phys. Rev. Lett. **102**, 103901 (2009).

[18] J. P. Farrell, L. S. Spector, B. K. McFarland, P. H. Bucksbaum, M. Gühr, M. B. Gaarde, and K. J. Schafer, Phys. Rev. A **83**, 023420 (2011).

[19] K.-H. Hong, C.-J. Lai, V.-M. Gkortsas, S.-W. Huang, J. Moses, E. Granados, S. Bhardwaj, and F. X. Kärtner, Phys. Rev. A **86**, 043412 (2012).

[20] S. Pabst, L. Greenman, D. A. Mazziotti, and R. Santra, Phys. Rev. A **85**, 023411 (2012).

[21] B. K. McFarland, J. P. Farrell, P. H. Bucksbaum, and M. Gühr, Science **322**, 1232 (2008).

[22] B. K. McFarland, J. P. Farrell, P. H. Bucksbaum, and M. Gühr, Phys. Rev. A **80**, 033412 (2009).

[23] M. Lewenstein, P. Balcou, M. Y. Ivanov, A. L'Huillier, and P. B. Corkum, Phys. Rev. A **49**, 2117 (1994).

[24] J. Itatani, J. Levesque, D. Zeidler, H. Niikura, H. Pépin, J. C. Kieffer, P. B. Corkum, and D. M. Villeneuve, Nature **432**, 867 (2004).

[25] A.-T. Le, X. M. Tong, and C. D. Lin, J. Mod. Opt. **54**, 967 (2007).

[26] X. Chu and S.-I. Chu, Phys. Rev. A **64**, 063404 (2001).

[27] X. Chu and M. McIntyre, Phys. Rev. A **83**, 013409 (2011).

[28] B. Zimmermann, M. Lein, and J. M. Rost, Phys. Rev. A **71**, 033401 (2005).

[29] M. Guhr, B. K. McFarland, J. P. Farrell, and P. H. Bucksbaum, J. Phys. B: At. Mol. Opt. Phys. **40**, 3745 (2007).

[30] P. Baltzer, M. Larsson, L. Karlsson, B. Wannberg, and M. C. Göthe, Phys. Rev. A **46**, 5545 (1992).

[31] X. Chu and S.-I. Chu, Phys. Rev. A **63**, 023411 (2001).

[32] X. Chu and S.-I. Chu, Phys. Rev. A **70**, 061402(R) (2004).

[33] D. A. Telnov and S.-I. Chu, Phys. Rev. A **80**, 043412 (2009).

[34] X. Chu, Phys. Rev. A **82**, 023407 (2010).

[35] X. Chu and P. J. Memoli, Chem. Phys. **391**, 83 (2011).

[36] E. Runge and E. K. U. Gross, Phys. Rev. Lett. **52**, 997 (1984).

[37] E. K. U. Gross and W. Kohn, Adv. Quant. Chem. **21**, 255 (1990).

[38] G. Vignale, Phys. Rev. A **77**, 062511 (2008).

[39] L. D. Landau and E. M. Lifshitz, *The Classical theory of fields* (Pergamon, Oxford, 1975), 4th ed.

[40] Y. Mairesse, J. Levesque, N. Dudovich, P. B. Corkum, and D. M. Villeneuve, J. Mod. Opt. **55**, 2591 (2008).

[41] X. Chu and G. C. Groenenboom, Phys. Rev. A **85**, 053402 (2012).

[42] We performed an internally contracted multireference singles and doubles excitation configuration interaction calculation with the MOLPRO [46] package. The orbitals were obtained with

a full valence state-averaged CASSCF calculation employing the aug-cc-pVQZ one electron basis.

[43] P. Cremaschi, A. Chattopadhyay, P. V. Madhavan, and J. L. Whitten, Chem. Phys. **109**, 117 (1986).

[44] A. Lofthus and P. H. Krupenie, J. Phys. Chem. Ref. Data **6**, 113 (1977).

[45] K. Wang, J. A. Stephens, and V. McKoy, J. Chem. Phys. **95**, 6456 (1991).

[46] H.-J. Werner, P. J. Knowles, and *et al.*, MOLPRO*: a package of ab initio programs, version 2010.1*, URL `http://www.molpro.net`.

[47] R. J. Le Roy, University of Waterloo, Chem. Phys. Res. Rep. No. **CP-657R** (2004), URL `http://leroy.uwaterloo.ca`.

[48] T. Trickl, D. Proch, and K. L. Kompa, J. Mol. Spectrosc. **171**, 374 (1995).

[49] R. A. Gottscho, R. W. Field, K. A. Dick, and W. Benesch, J. Mol. Spectrosc. **74**, 435 (1979).

[50] D. T. Colbert and W. H. Miller, J. Chem. Phys. **96**, 1982 (1992).

[51] G. C. Groenenboom and D. T. Colbert, J. Chem. Phys. **99**, 9681 (1993).

Table I: Vertical ionization potentials of $N_2$, the experimental value [30], the *ab initio* value (MRCI) [42], and the DFT value (see Sec. IV). Column five gives the dominant excitation with respect to the ground state of the ion and the excitation energy $\Delta E_{exc}$ is estimated from DFT calculations.

| | $I_p$ (eV) | | | resonance | | excitation | | | |
|---|---|---|---|---|---|---|---|---|---|
| Ionic state | experiment | MRCI | DFT | $\theta$ | $\hbar\omega$ (eV) | assignment | | | $\Delta E^{\rm ion}_{\rm exc}$ (eV) |
| $X\,^2\Sigma_g^+$ | 15.580 | 15.406 | 15.580 | | | | | | |
| $A\,^2\Pi_u$ | 16.926 | 16.912 | 16.863 | 90° | ∼17 | $1\pi_u$ | → | $3\sigma_g$ | 1.283 |
| $B\,^2\Sigma_u^+$ | 18.751 | 18.569 | 18.700 | | | $2\sigma_u$ | → | $3\sigma_g$ | 3.120 |
| $2\,^2\Pi_g$ | 24.788 | 24.547 | 23.518 | | | $3\sigma_g$ | → | $1\pi_g$ | 7.938 |
| $C\,^2\Sigma_u^+$ | 25.514 | 25.321 | 24.802 | 0° | 23–26 | $1\pi_u$ | → | $1\pi_g$ | 9.222 |
| $D\,^2\Pi_g$ | (26) | 26.064 | 26.085 | | | $1\pi_u^2$ | → | $3\sigma_g\,1\pi_g$ | 10.505 |
| $2\,^2\Pi_u$ | (30) | 28.326 | 26.639 | 90° | 26–30 | $2\sigma_u$ | → | $1\pi_g$ | 11.059 |
| $F\,^2\Sigma_g^+$ | 28.8 | 28.864 | 27.922 | | | $2\sigma_u\,1\pi_u$ | → | $3\sigma_g\,1\pi_g$ | 12.342 |

Table II: Orbital energies ($\epsilon$) of $N_2$ calculated with the $LB_\alpha$ potential, and the ground state occupation.

| Orbital | $\epsilon$ (eV) | occupation |
|---|---|---|
| $2\pi_u$ | −2.910 | 0 |
| $3\sigma_u$ | −2.966 | 0 |
| $4\sigma_g$ | −3.730 | 0 |
| $1\pi_g$ | −7.642 | 0 |
| $3\sigma_g$ | −15.580 | 2 |
| $1\pi_u$ | −16.863 | 4 |
| $2\sigma_u$ | −18.700 | 2 |

Table III: Two-center interference minimum predicted by Eq. (34), Eq. (33), and the TDDFT calculation, together with the harmonic order (HO) from the TDDFT calculation.

| | $\hbar\omega_{min}$ (eV) predicted by | | | |
|---|---|---|---|---|
| R ($a_0$) | Eq. (34) | Eq. (33) | TDDFT | HO |
| 2.7 | 18.420 | 22.986 | 23.25 | 15 |
| 2.6 | 19.864 | 25.002 | 26.35 | 17 |
| 2.5 | 21.485 | 27.264 | 26.35 | 17 |
| 2.3 | 25.384 | 32.690 | 32.55 | 21 |
| 2.2 | 27.744 | 35.955 | 35.65 | 23 |
| 2.1 | 30.450 | 39.672 | 38.75 | 25 |
| 2.0 | 33.5707 | 43.920 | 44.95 | 29 |
| 1.9 | 37.198 | 48.799 | 48.05 | 31 |

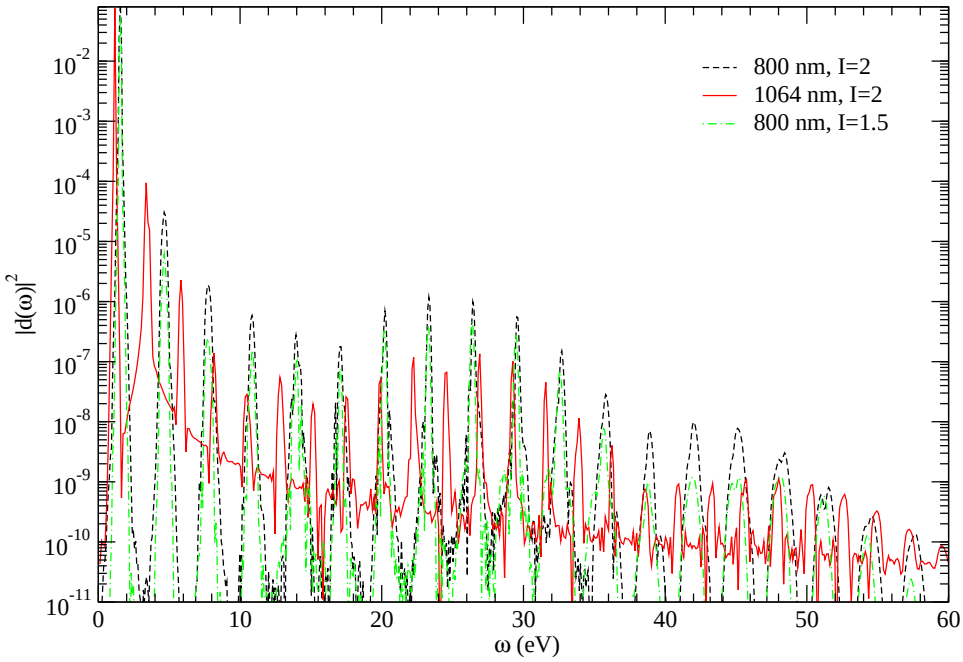


Figure 1: (Color on line) The HHG of $N_2$ at the equilibrium geometry calculated with the TDDFT method. The unit for laser intensity $I$ is $10^{14}$ W/cm$^2$ and the pulse length is 20 optical cycles. The wavelengths are $\lambda = 800$ nm (black dashed line and green dot-dash line) and $\lambda = 1064$ nm (red solid line).

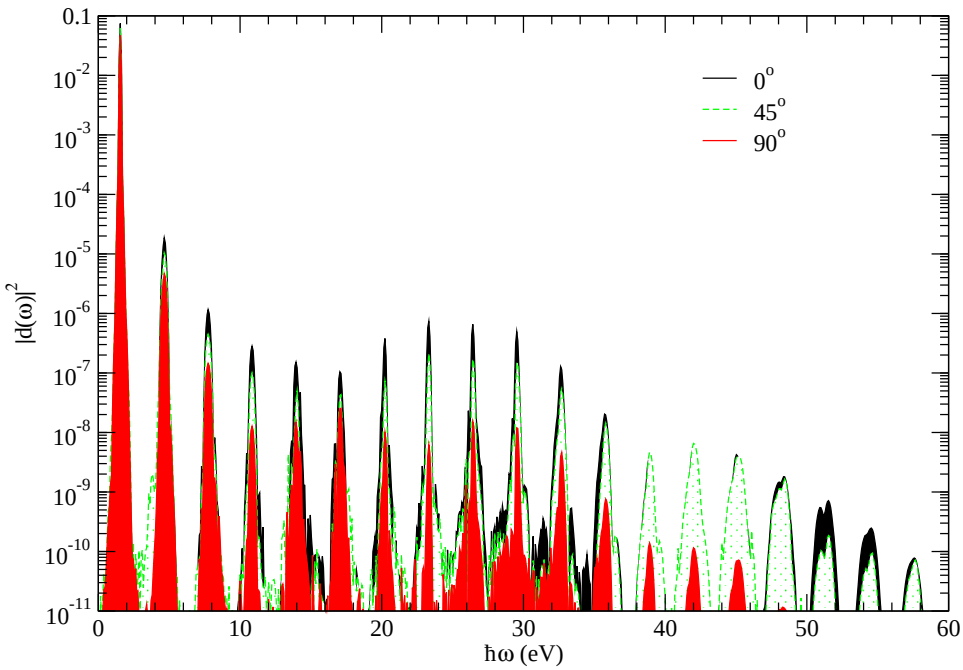


Figure 2: The HHG of $N_2$ calculated with the TDDFT method. The laser intensity is $2\times10^{14}$ W/cm$^2$ and the pulse length is 20 optical cycles. The orientation angles are $\theta = 0°$ (black solid line), $\theta = 45°$ (red dashed line), and $\theta = 90°$ (green solid line).

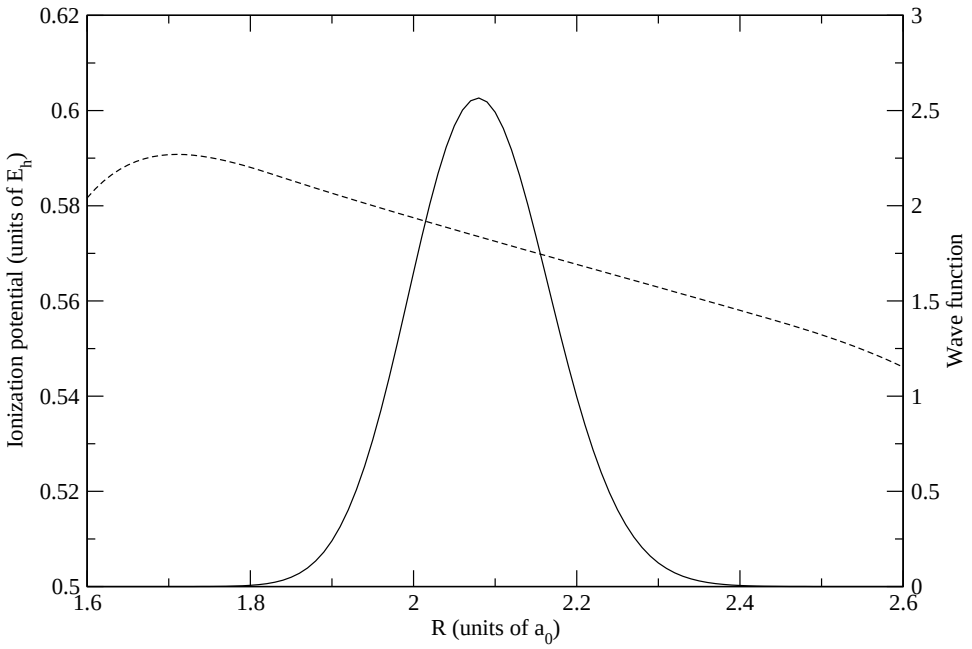


Figure 3: The ionization potential of $N_2$ as a function of $R$ calculated with the Rydberg-Klein-Rees method [47] with spectroscopic data for $N_2$ and $N_2^+$ from Refs. [48] and [49], respectively (black dashed line) and the ground state vibrational wave function $\chi_0(R)$ computed with the sinc-function discrete variable representation method [50, 51] (black solid line).

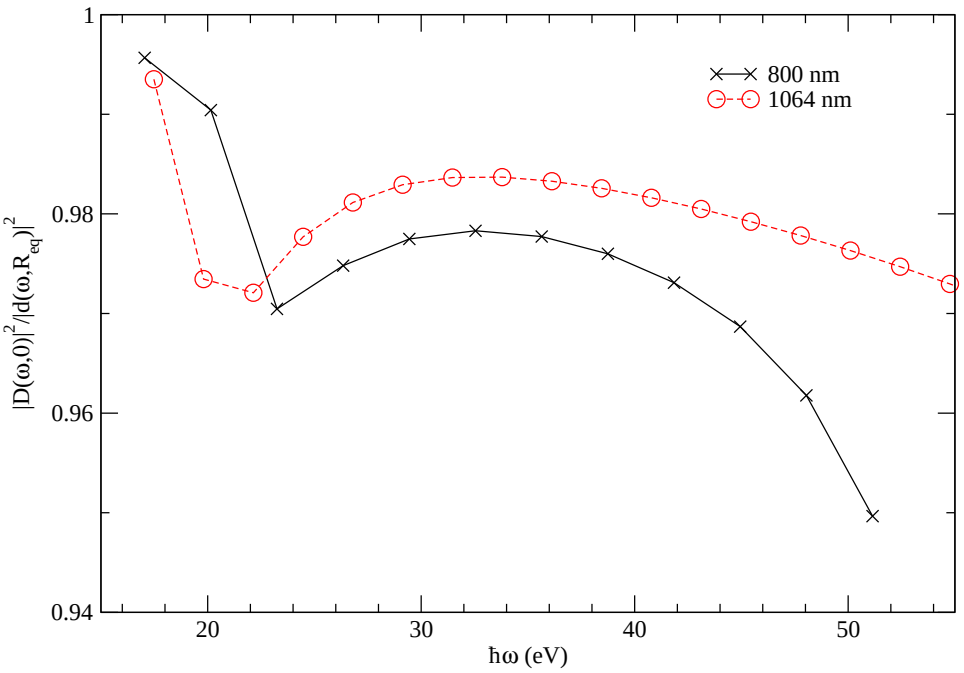


Figure 4: (Color on line) Ratio of the HHG intensity calculated with Eq. (13) for the ground vibrational state and by fixing the internuclear distance at $R_e$. The laser intensity is $2\times10^{14}$ W/cm$^2$ and $\theta = 0°$.

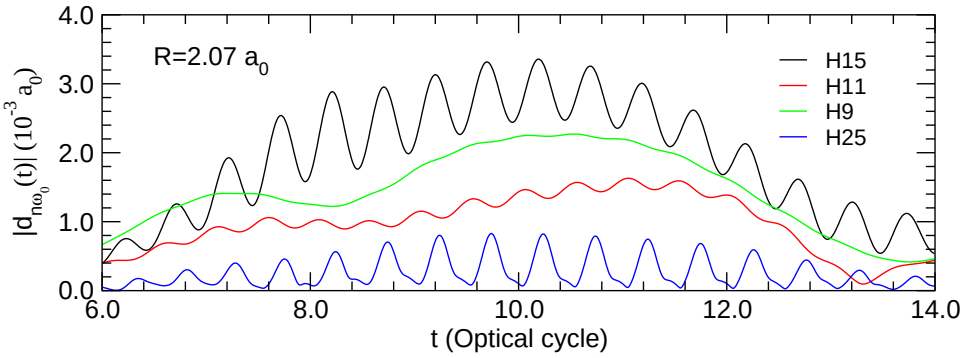


Figure 5: Time profiles of the 9th, 11th, 15th, and 25th harmonic for $R = R_e = 2.07\ a_0$, and the 15th, 19th, and 11th harmonic for $R = 2.7\ a_0$. The laser intensity is $2\times10^{14}$ W/cm$^2$ and $\theta = 0°$.

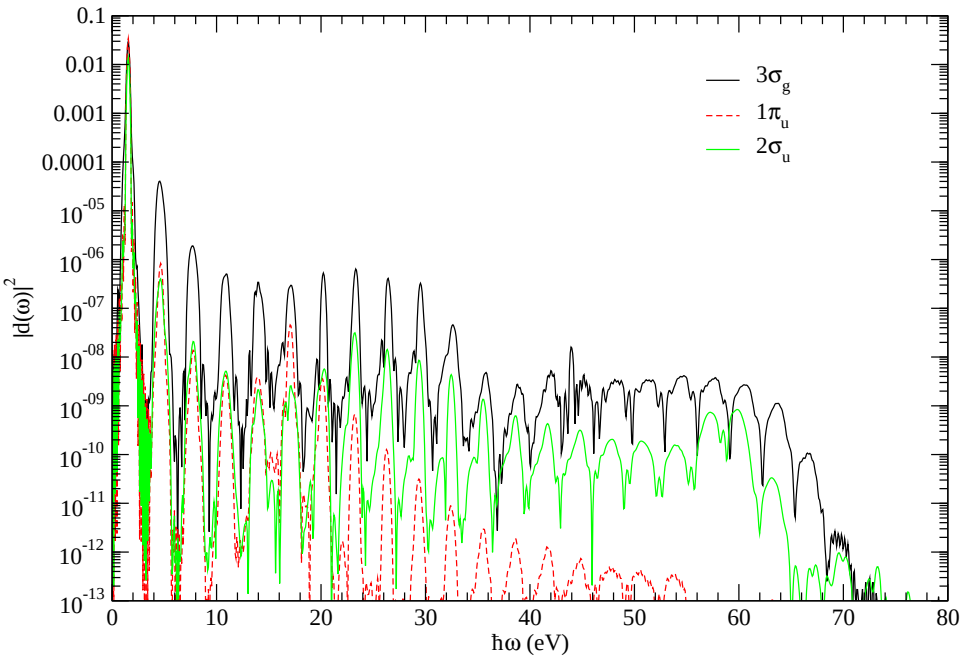


Figure 6: Contribution of individual initially occupied orbitals to HHG, obtained by freezing all other occupied orbitals. The laser intensity is $2\times10^{14}$ W/cm$^2$ and $\theta = 0°$.

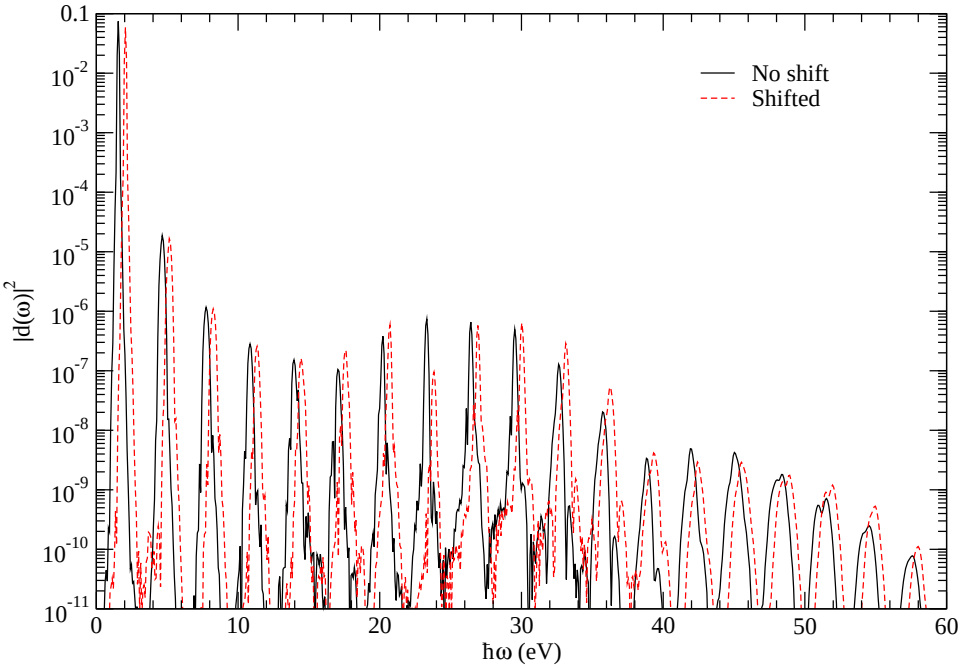


Figure 7: (Color on line) Effect of shifting the energy of the unoccupied $1\pi_g$ orbital up by 0.25 $E_h$ (6.8 eV). The laser intensity is $2\times10^{14}$ W/cm$^2$ and $\theta = 0°$.

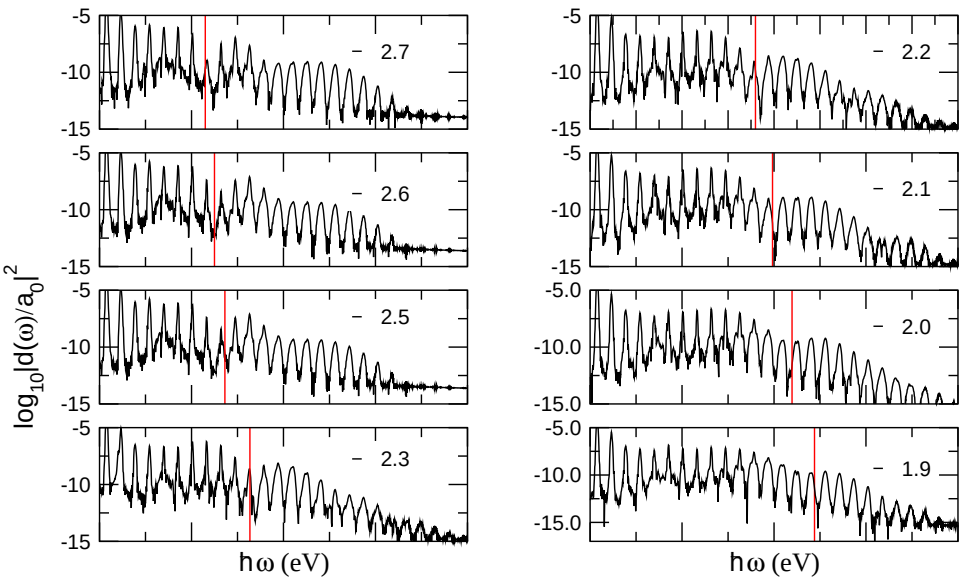


Figure 8: The HHG of $N_2$ at a series of internuclear distances calculated with the TDDFT method. The distances are labeled for each spectrum. The laser intensity is $2\times10^{14}$ W/cm$^2$ and the pulse length is 20 optical cycles. The wavelengths are $\lambda = 800$ nm (black solid line). The molecular axis is parallel to the polarization direction of the field. The positions of the minima predicted by the modified two-center interference model are shown by vertical red solid lines.